NJC

New Journal of Chemistry

An international journal of the chemical sciences

www.rsc.org/njc

Volume 33 | Number 5 | May 2009 | Pages 921–1156

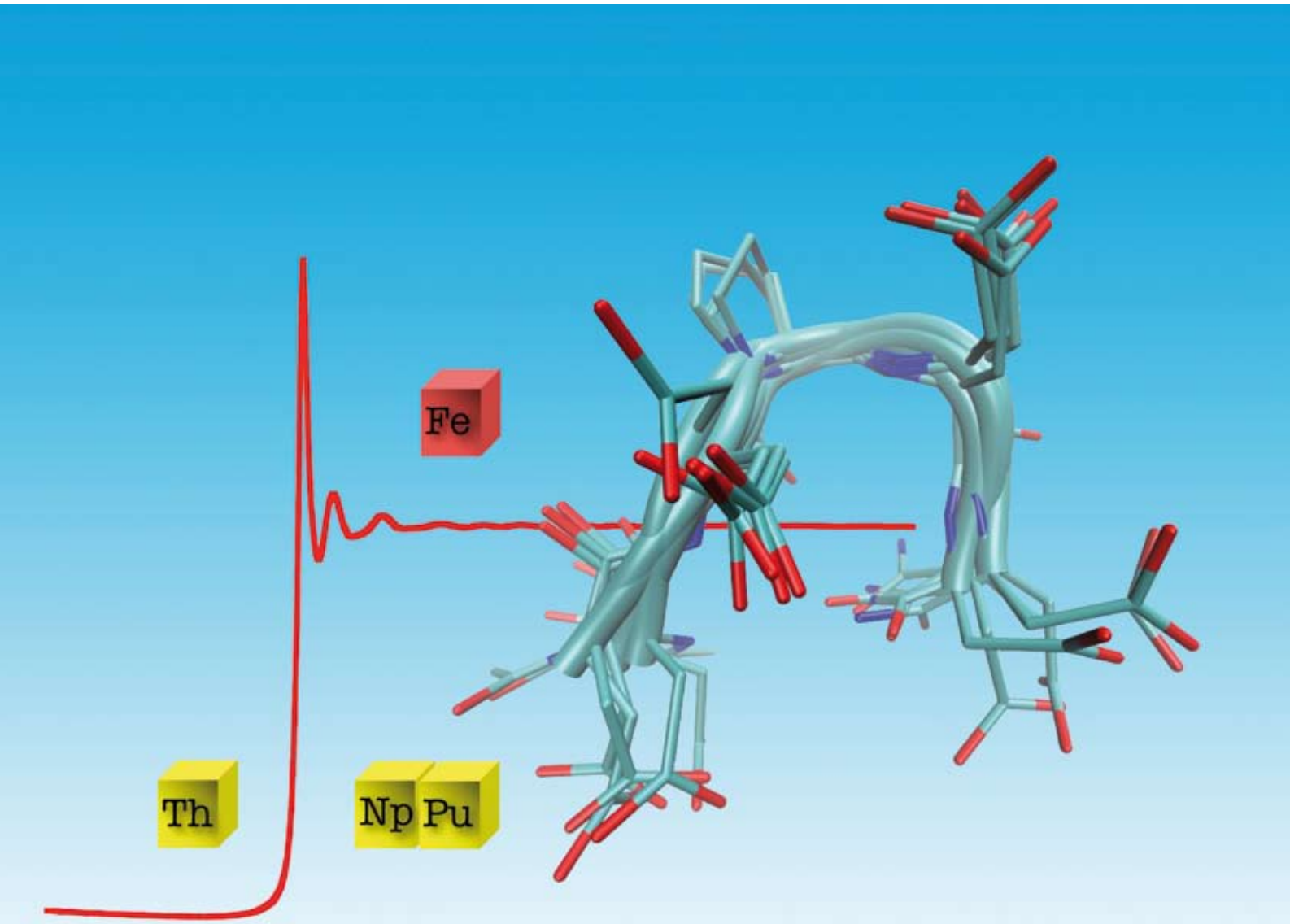

ISSN 1144-0546

RSC Publishing

PAPER

Christophe Den Auwer *et al.*

The role of aspartyl-rich pentapeptides in comparative complexation of actinide(IV) and iron(III). Part 1

1144-0546(2009)33:5;1-Z

The role of aspartyl-rich pentapeptides in comparative complexation of actinide(IV) and iron(III). Part 1

Aurélie Jeanson,[a] Claude Berthon,[a] Stéphanie Coantic,[bcd] Christophe Den Auwer,*[a] Nicolas Floquet,[c] Harald Funke,[e] Denis Guillaneux,[a] Christoph Hennig,[e] Jean Martinez,[c] Philippe Moisy,[a] Sébastien Petit,[a] Olivier Proux,[f] Eric Quémeneur,[b] Pier Lorenzo Solari[g] and Gilles Subra[c]

Received (in Montpellier, France) 5th August 2008, Accepted 11th December 2008
First published as an Advance Article on the web 26th January 2009
DOI: 10.1039/b813523a

Although there is a tremendous volume of data available on the interaction of actinides with living organisms as plants, nearly all the studies are limited to macroscopic or physiological measurements with no specific information at the molecular level. Peptides allow the study of complex coordination chemistry, as that involving actinide(IV) and proteins, without the intricacy of tertiary structure properties. For that purpose, a linear pentapeptide, acetyl–diaspartyl–prolyl–diaspartyl–amide (Ac–Asp–Asp–Pro–Asp–Asp–NH_2, denoted PP1 in this report), was synthesized and investigated as a potential chelating ligand of thorium(IV), neptunium(IV) and/or plutonium(IV) cations. Comparison with the biological relevant iron(III) cation is also provided. Noteworthy, PP1 was able to prevent Np(IV) from hydrolysis into an insoluble precipitate. Spectrophotometry, ^{13}C NMR and EXAFS at the iron K edge and actinide L_3 edges were used to probe the cation coordination sphere and better describe the cation–peptide interaction. The complexes were found to be polynuclear with oxo or hydroxo bridged cations, Fe(III) forming a binuclear complex, Th(IV), Np(IV) or Pu(IV) forming a polynuclear complex with higher nuclearities.

Introduction

Most data available on the interaction of actinides with biological systems are based on macroscopic measurements, with very little structural information at the molecular level. However, in case of accidental release of radionuclides, internal contamination with actinides (Th, U, Np, Pu, Am) under either acute or chronic conditions has the potential to induce both radiological and chemical toxicity. Whatever the route of contamination (inhalation, ingestion or wound), the radionuclide is absorbed into, and then transported by blood with absorption rate depending on the dissolution properties of the initial physico-chemical form. It is then deposited in the target organs (*e.g.* bone, kidney, liver) in which it is stored and then slowly eliminated through urine and faeces. For instance Pu(IV) retention in the human body is 50% in bone and 30% on liver.[1] Although there is a tremendous volume of data available on the interaction of plutonium with living organisms such as plants, nearly all the studies are limited to macroscopic or physiological measurements with no specific information at the molecular level. Molecular approaches have been very seldom used due to the combined intricacy of metallo biochemistry and actinide chemistry.[2] However, such "molecular speciation" related to actinide in biomolecules is of considerable interest to understand the potential transport of radionuclide inside living organisms. It also has an important input in providing guidance on the structure, affinity and design of potential specific chelating agents synthesized and used for the elimination of incorporated radionuclides.

One of the strategies to understand the interaction of actinide elements with biomolecules is to consider metallobiomolecules as elaborated coordination complexes with well-designed metal active sites. Comparison with biorelevent "analogues", such as Fe(III) has revealed a very promising tool in order to rationalize the selective propensity of organic ligands to chelate actinide cations. More generally, a spread belief is that the coordination properties of some actinides at oxidation state +IV (Th, Np, Pu) in biological systems compares with that of iron, particularly Fe(III). For instance, the chemical similarity between Pu(IV) and Fe(III) has been observed in the siderophore-mediated uptake of Pu by *Microbacterium flavescens*[3] or in the transferrin system.[4] But, in fact, very few studies have directly addressed this issue with biomimetic compounds.

Actinide elements display a very rich chemistry because of the specific properties of their 5f and 6d valence electrons. At oxidation state +IV, actinides behave mostly as hard acids in

[a] *CEA Marcoule DEN/DRCP/SCPS, 30207, Bagnols sur Cèze, France. E-mail: christophe.denauwer@cea.fr*
[b] *CEA Marcoule DSV/iBEB/SBTN, 30207, Bagnols sur Cèze, France*
[c] *Institut des Biomolécules Max Mousseron, CNRS UMR-5247, Université Montpellier I-II, 34093, Montpellier, France*
[d] *ICSM Marcoule UMR 5257, 30207, Bagnols sur Cèze, France*
[e] *Forschungzentrum Dresden–Rossendorf, Institute of Radiochemistry, D-01314 Dresden, Germany*
[f] *Laboratoire de Géophysisque Interne et Technophysique, UMR CNRS/Université J. Fourier, 38400, Saint Martin d'Hères, France*
[g] *Synchrotron SOLEIL, MARS beam line, 91192, Gif sur Yvette, France*

the Pearson classification, resulting in strong interactions with hard donor groups such as carboxylates. Although their ability for complexation is relatively high compared to oxidation state +III, their tendency to hydrolysis is also very strong, often resulting in mixed hydroxy species when dealing with physiological conditions.[5] In case of internal contamination, various studies have shown the affinity of actinides with transferrin, calmodulin or albumin metalloproteins. Indeed, it has been suggested that actinide(IV) ions were chelated in the iron complexation site of the transferrin,[6] composed of two tyrosines, one histidine and one aspartic acid. Concerning actinide–calmodulin interaction, it has been brought to light that plutonium(III) binds specifically in the calcium binding site,[7] constituted of five oxygen atoms from the side chain of aspartate and glutamate amino acids and one oxygen atom from the carbonyl group of a peptide bound. Moreover, a screening of structures of uranyl–protein complexes in the Protein Data Bank (PDB) has been carried out by Van Horn *et al*.[8] The coordination donors include aspartyl and glutamyl carboxylate, tyrosinate and amide oxygen atoms. Acidic amino-acids (Asp and Glu) or the free carboxylate terminus are indicated as binding uranium in most of the reported structures. Pible *et al*. have recently developed an *in silico* method in order to localize possible complexation sites of uranyl in 3D-structures of proteins.[9] This study unsurprisingly brings out that oxygen atoms are the preferential ligands for uranyl, with a mean distance of 2.51 Å. Among the amino-acids considered as the most favourable to uranyl chelation are aspartic and glutamatic acids (with the two oxygen atoms of their carboxylate function), and tyrosine, serine and threonine (with their hydroxide function). All these metal binding sites involve carboxylate functional groups from aspartic amino acid residues.

Our approach in the first step of this work is to consider simple organic ligands that bear some of the functional groups of a protein binding site without the intricacy of tertiary structure properties. A simple linear pentapeptide, acetyl–aspartyl–aspartyl–prolyl–aspartyl–aspartyl–amide (Ac–Asp-Asp-Pro-Asp-Asp–NH_2, denoted PP1), was then chosen as a model. This particular candidate presents several advantages: (i) the proline residue defines a symmetric peptide with some allowed flexibility and potential turn[10,11] facilitating the interaction of aspartate side chain with cations, albeit the short length might moderate tertiary effects in a rough approximation; (ii) comparison between carboxylate functions engaged in a small peptidic chain and carboxylic acids is facilitated by the large number of crystal structures available in the literature of actinide(IV)–carboxylate complexes, (iii) the peptide size is small enough to neglect in a first approximation tertiary structural effects. Furthermore, related aspartyl-rich di- and tripeptides have already been reported to bind Al(III) cation.[12]

In this paper, we report our first results on the interaction between actinide(IV) (thorium, neptunium, plutonium) and aspartyl pentapeptides in aqueous solution. The paper is structured the following way: in the results part, data from local spectroscopic probes are reported. Among these techniques, X-ray absorption spectroscopy (EXAFS) is the central tool of this study. It is a local, element specific structural probe that has been increasingly applied to metal centers in biological systems but also to actinides in solution.[13,14] Then, we propose a structural model for the interaction between Ac–AspAspProAspAsp–NH_2 and actinide(IV) and iron(III) cations. This model is further discussed in the light of theoretical calculations based on the Fe(III)–Ac–AspAspProAspAsp–NH_2 system.

Experimental

Spectrophotometry

The spectra of aqueous solutions of Fe(III) complexes were recorded on a Cary 500 UV-visible spectrophotometer in the range 200–700 nm, using 1 cm quartz cells. The sampling interval was fixed at 0.5 nm.

Measurements of actinide samples were carried out on a Schimadzu 3101 spectrophotometer at room temperature, with a 0.1 cm path length quartz cell. The sampling interval was fixed at 1 nm, with a slit width of 0.8 nm.

Stock solutions of ferric and actinide cations

$FeCl_3{\cdot}6H_2O$ was provided by Merck. The stock solution of Fe(III) ([Fe] = 0.1 M) was obtained by dissolution of $FeCl_3{\cdot}6H_2O$ in water. Actinide starting materials were obtained from the CEA inventory. Actinides are radioactive elements and were handled in dedicated glove boxes. Plutonium (^{239}Pu) and neptunium (^{237}Np) were purified by ion exchange on an anionic resin AGMP1 (Dowex). The stock solution of Np(IV) ([Np] = 50 mM) was prepared by hydroxylammonium chloride (250 mM) reduction (70 °C) of a Np(V) solution previously obtained by dissolution of $Np(V)O_2OH{\cdot}xH_2O$ ($x \approx 2.5$) in hydrochloric acid ($\approx$1 M). The reaction was monitored by spectrophotometry in order to control neptunium concentration, and to insure that less than 1% Np(V) remained in the solution. The stock solution of Pu(IV) ([Pu] = 32 mM) was prepared in nitric acidic solution (0.55 M). Solid thorium nitrate $Th(NO_3)_4{\cdot}5H_2O$ (Prolabo) was used without further purification. The stock solution of Th(IV) ([Th] = 20 mM) was obtained by dissolution of thorium nitrate into 0.1 M hydrochloric acidic.

Synthesis of Ac–Asp–Asp–Pro–Asp–Asp–NH_2 (PP1)

Unless otherwise noted, solvents and reagents were obtained from commercial suppliers and used without further purification. The Fmoc and side-chain protected amino acids (Fmoc–Asp(OtBu)–OH, Fmoc–Pro–OH) and the Polystyrene Rink Amide resin (bead diameter 75–150 μm and substitution 0.7 mmol g^{-1}) were provided by Iris Biotech GmbH. Peptides were synthesized manually by standard Fmoc chemistry using *N*-hydroxybenzotriazole (HOBT) and *N*,*N*′-diisopropylcarbodiimide (DIPCDI) as activation reagents.

Fmoc-deprotection protocol. The Fmoc-deprotection step was carried out by suspending the resin in a mixture of piperidine and dimethylformamide (DMF) (1 : 4, v/v) for 20 min. After removal of the deprotection solution, the resin was washed with DMF (twice) and dichloromethane (DCM) (twice).

Coupling protocol. DMF solutions containing Fmoc-amino acid (4 eq.; 0.2 M), HOBT (4 eq.; 0.2 M) and DIPCDI (4 eq.; 200 mM) were freshly prepared before coupling. The resins were suspended for 1–2 h in the coupling solution at room temperature. The solution was filtered and the resin was washed twice with DMF and then twice with DCM.

Acetylation. *N*-Terminal acetylation was performed by using an excess of acetic anhydride in DCM (1 : 1, v/v) for 5 min (twice). The resin was washed with DCM (twice).

Synthesis. 700 mg of Fmoc-Rinkamide PS Resin give after SPPS, cleavage/deprotection and purification, 210 mg of peptide Ac–AspAspProAspAsp–NH_2 (69% yield, 97% purity). HPLC rt 0.76 min^{-1}; MS (ESI) *m*/*z* (rel. intensity, %) 655.3 ($[M + K]^+$, 8%), 639.5 ($[M + Na]^+$, 65%), 617.3 ($[M + H]^+$, 100%).

LC/MS purification. Crude peptide product obtained after cleavage was purified using an LC/MS autopurification system consisting of a binary pump Waters 2525, an injector/fraction collector Waters 2676, coupled to a Waters Micromass ZQ2000 Spectrometer (electrospray ionisation mode, ESI+). All the purifications were carried out using a Waters Symmetry Shield C18, 19 × 100 mm, 5 μm particle size, column. A flow rate of 20 mL min^{-1} and a gradient of 0–60% of B over 20 min were used. Solvent A was 0.1% TFA in water, and solvent B 0.1% TFA in acetonitrile. Positive-ion electrospray mass spectra were acquired at a solvent flow rate of 204 μL min^{-1}. Nitrogen was used for both the nebulizing and drying gas. The data were obtained in a scan mode ranging from 100 to 1000 *m*/*z* in 0.1 s intervals; 10 scans were summed up to get the final spectrum. Collection control trigger was set on single protonated and diprotonated ion with minimum intensity threshold of 8×10^5. Fractions with the correct peptide were pooled and lyophilized to provide white powder.

Analytical HPLC. This was performed on a Waters 996 system with a diode array detector (purity check at 214 nm) and a Chromolith SpeedRod C_{18} column (4.6 × 50 mm). (solvent A: water–0.1% TFA, solvent B: acetonitrile–0.1% TFA). The gradient was 100% A to 100% B in 3 min (flow rate 5 mL min^{-1}).

LC/MS analysis. The LC/MS system consisted of a Waters Alliance 2690 HPLC, coupled to a Micromass Quatro Micro spectrometer (electrospray ionization mode, ESI+). All analyses were carried out using a Chromolith Flash $RP_{18}E$ column (4.6 × 25 mm). A flow rate of 1.5 mL min^{-1} and a gradient of 100% A to 100% B over 4 min were used (solvent A: water–0.1% HCOOH, solvent B: acetonitrile–0.1% HCOOH).

Fe(III)–PP1 complex

Iron complexes were prepared in water, by direct addition of appropriate volumes of the iron stock solution into a solution of PP1 (pH = 5). Table 1 summarizes the sample compositions studied in this report.

An(IV)–PP1 complex (An = Th, Np, Pu)

All actinide samples were prepared in water, in the presence of acido-basic buffer *N*-(2-hydroxyethyl)piperazine-*N*′-(2-ethanesulfonic acid) (HEPES, provided by Sigma-Aldrich), by slowly adding the actinide solution in a PP1 solution ([PP1] = 50 mM), then diluting in HEPES solution ([HEPES] = 250 mM). When necessary, pH adjustment was fulfilled with ammonia. Table 1 summarizes all the sample compositions.

NMR of free PP1 and Th–PP1 complex

NMR spectra were recorded on a Varian Unity INOVA 400 MHz spectrometer equipped with a 5 mm PFG tunable triple resonance indirect detection $^1H\{^{13}C/X\}$ probe.

^1H and ^{13}C signals of metal-free PP1 peptide were collected at 17 mM in water (pH = 4). The water proton signals were intense and saturated the detector (gain around 25), so preventing a good detection of the PP1 signals. Thus, a 1.5 s rectangular selective pulse was added at the beginning of gHSQC and gHMBC sequences in order to saturate the signal from water, resulting in a maximum receiver gain (60 dB).

The titration by NMR of the formation of the Th–PP1 complex was performed at 7.5 mM PP1 in 0.1 M HEPES, pH 7.0. In that case, samples were analyzed in a double-layer tube (Teflon liner inserted in a 5 mm screw-capped glass tube). Acetone-D_6, used as lock solvent and reference for the ^1H and ^{13}C chemical shifts was inserted between the glass tube and the Teflon liner. As the samples were concentrated in HEPES, strong signals from the HEPES protons appeared between 2 and 4 ppm. These signals added to the protons signals from water molecules induced the saturation of the detector. Then, a train of shaped pulses lasting 1.5 s (the pulse shape created with PBox is made of several *e-burp* pulses with offsets and widths corresponding to each strong hydrogen signal from water and HEPES) was added at the beginning of gHSQC and gHMBC sequences. In these conditions, the receiver gain reached the maximum value (60 dB).

EXAFS data acquisition, processing and analysis

Data acquisition and processing. EXAFS spectra were recorded at the European Synchrotron Radiation Facility (ESRF) (6 GeV at 200 mA) and at the Stanford Synchrotron Radiation Laboratory (SSRL) (3 GeV at 100 mA).

Iron K-edge EXAFS spectra were recorded at the French Absorption spectroscopy beam line in Material and Environmental science (FAME, BM30b) of the ESRF. FAME is equipped with a liquid-nitrogen cooled double-crystal Si(220) monochromator. Higher harmonics were rejected by two focusing rhodium coated mirrors. A 30-element Ge solid state detector was used for data collection in the fluorescence mode. Monochromator energy calibration was carried out at iron K-edge (7112 eV at the inflection point). Measurements were carried out at room temperature, in 200 μL Teflon cells.

Thorium and plutonium L_{III}-edge EXAFS spectra were recorded at the Rossendorf beam line of the ESRF (BM20). BM20 is equipped with a water-cooled double-crystal Si(111) monochromator. Higher harmonics were rejected by two collimating Pt coated mirrors. A 13-element Ge solid-state detector was used for data collection in the fluorescence mode.

Table 1 Sample composition for the synthesis of the Fe–PP1 and An–PP1 (An = Th, Np, Pu) complexes (EXFAS: extended X-ray absorption fine structure, MS: mass spectrometry, UV: UV-visible spectrophotometry)

Sample name	Exp. techniques	Composition [Fe]/[PP1] (mM)	M : PP1 ratio	pH
Fe–PP1	EXAFS + UV	50.0/88.2	1 : 1.8	4.0
Fe–PP1–MS	MS + UV	1.0/1.0	1 : 1.0	5.0
Fe–PP1–UV	UV	0.02/0.08	1 : 4.0	5.0
Th–PP1	EXAFS + UV	5.0/10.3	1 : 2.0	4.0
Th–PP1–NMR	NMR + UV	7.5/7.5	1 : 1.0	7.0
Np–PP1-0.7	UV	5.0/3.5	1 : 0.7	1.5
Np–PP1-0.9	UV	4.8/4.3	1 : 0.9	1.5
Np–PP1-1.5	EXAFS + UV	6.5/9.7	1 : 1.5	1.5
Np–PP1-5.5	UV	3.8/20.9	1 : 5.5	1.5
Np–PP1-7.5	EXAFS + UV	6.5/48.7	1 : 7.5	1.5
Np–PP1-23	EXAFS + UV	5.0/119.0	1 : 23	1.5
Np–PP1-pH5	EXAFS + UV	9.7/9.7	1 : 1.0	5.5
Np–PP1-pH8	EXAFS + UV	9.7/9.7	1 : 1.0	8.3
Pu–PP1	EXAFS + UV	5.0/9.8	1 : 2.0	1.5

Neptunium L_{III}-edge EXAFS spectra were recorded on beam line 11-2 of SSRL. The beam line is equipped with a liquid-nitrogen cooled double-crystal Si(220) monochromator, and with two collimating and focusing rhodium coated mirrors. A 30-element Ge solid-state detector was used for data collection in the fluorescence mode.

Monochromator energy calibration of the actinide absorption spectra was carried out at yttrium K-edge (17 052 eV at the absorption maximum). All measurements were recorded in double-layered cells of 200 μL specifically designed for radioactive samples, at room temperature.

Data were processed using the Athena code.[15] Background removal was performed using a pre-edge linear function. Atomic absorption was simulated with a cubic spline function.

Data fitting. The extracted EXAFS signal was fitted in *R* space without any additional filtering using the ARTEMIS code.[15] All adjustments were performed between 1 and 5 Å. Only single-scattering paths were considered. The *R* factor and quality factor $\Delta\chi^2_\nu$ are both provided as an indication of the fit quality in *R* space while the average noise of the spectrum ε was estimated with back Fourier transformation in $k^3\chi(k)$ mode above 6 Å with the Cherokee code.[16] In all the fits, only one global amplitude factor and one energy threshold factor were considered for all the contributions.

Fe–PP1 (Kaiser window = 2.2–12.9 Å^{-1}, fit range = 1–5 Å). Phases and amplitudes were calculated by the Feff82 code[17] from a Fe(III)-acetato cluster based on the crystallographic structure of a Fe(III)-acetato cluster, $[Fe_3O(CH_3COO)_6(H_2O)_3]NO_3{\cdot}4H_2O$ (CDB reference: LERZUD).[18] Two oxygen contributions, one shell of carbon atoms and one shell of Fe in the single-scattering approximation were included in the fitting procedure. The XANES spectrum of Fe K edge showed that iron fitted in an octahedral coordination sphere. Thus, the numbers of oxygen atoms of the two shells were linked together, setting the sum to six, and linked to the number of neighboring iron atoms. The number of carbon atoms was fitted freely.

Th–PP1, Np–PP1 and Pu–PP1 complexes (Kaiser window = 1.8–11.0, 1.8–10.7 and 1.8–10.9 Å^{-1}, respectively, fit range = 1–5 Å). Phases and amplitudes were calculated by the Feff82 code from a Ce(III)-acetato cluster based on the crystallographic structure of a Ce(III)-acetato cluster $K[Ce(CH_3COO)_3]{\cdot}H_2O$ (CDB reference: KPACCE10).[19] The scarcity of an adequate polynuclear model compound has led us to artificially modify the crystal structure using CrystalMaker, assembling two $Ce(CH_3COO)_3$ moieties to form a binuclear complex in order to get a realistic An–An phase and amplitude. Two oxygen contributions, two shells of carbon atoms and one shell of An (An = Th, Np, Pu, respectively) in the single-scattering approximation were included in the fitting procedure. The numbers of oxygen atoms from the two first shell contributions were linked together, setting the sum to nine, and linked to the number of neighboring actinide atoms in a way described in the results section. The number of carbon atoms was fitted freely, with the same Debye–Waller factor for all the carbon shells used in the fit.

Simulation of the Fe–PP1 complex by molecular dynamics

For all simulations the CHARMM force field (PARAM SET 22) and program (version c34b1) were used.[20,21] Parameters for Fe^{3+} were kindly provided by Johan Bredenberg, computer modelling group, Karolinska Institute. The PP1 peptide was built with non charged extremities and with a *trans*-Pro3 residue. Molecular dynamics simulations were performed for the Fe–PP1 complex system using experimental data as distance constraints (*e.g.* Fe^{3+}/Fe^{3+}, Fe^{3+}/OH (oxygen) and Fe^{3+}/Asp(Oδ) constrained at 3.3, 1.9 and 2.1 Å, respectively). Each possible pair of Asp residues was tested as complexing the Fe^{3+} (*e.g.* Asp1/Asp2, Asp1/Asp4, …, Asp4/Asp5). The peptide was built with either all or the two aspartyl residues not complexing the Fe^{3+} deprotonated. In each case, the energy of the starting conformation was first minimized including the constraints and a 100 ns molecular dynamics simulation was produced *in vacuo* with a dielectric constant set to 80.0; a time step of 1 fs was used without any cutoff for the calculations of van der Waals or electrostatic interactions. The objective of these simulations was to produce as many models as possible of the peptide around the ionic system. For each trajectory a clustering procedure was further employed to reduce the entire set of conformations (10 000) to a desired number of clusters (50 for each trajectory); the clustering

approach consisted to fit all the snapshots of the trajectory either on the Fe^{3+} atoms or on the peptide backbone atoms and compute a 2D RMSD map for the peptide, comparing each pair of snapshots. An ascendant hierarchical clustering procedure was finally employed to extract the 50 most representative conformations of each trajectory. The energies of the 50 final solutions of each of the 12 trajectories were finally minimized without any constraints and the energies of the resulting structures were compared to each other. The isolated PP1 peptide was also studied in the same conditions. 3D density maps and graphical representations were computed with VMD.[22]

Results

Mass spectrometry of the Fe–PP1 complex

To confirm the formation of a new Fe–PP1 complex, the solution of Fe(III) and peptide with a 1 : 1 stoichiometry was analyzed by mass spectrometry. As shown in Fig. 1, the main signal observed corresponds to m/z = 705.7. This isotopic massif at m/z = 705.7 corresponds to a state of charge 2+. Moreover, the ion m/z = 716.7 may be attributed to the sodium adduct of the same complex [$2Fe^{3+}$, $4H_2O$, 2PP1, $-5H^+$, Na^+]$^{2+}$. The mass increment of 716.7 − 705.7 = +11 is characteristic of a dicharged sodium adduct. This data, combined to the different masses of the species in the medium, suggest that the Fe(III)–PP1 complex has a 2 : 2 stoichiometry. Nevertheless, MS/MS fragmentation gave no further indication about the structure of the complex, as the main fragment observed was free PP1.

Spectrophotometry of the Fe–PP1, Np–PP1 and Pu–PP1 complexes

UV-visible-NIR spectrophotometry is a local probe of the cation and peptide environments. Fig. 2 shows the absorption spectra of the complexes formed after addition of an excess of peptide over cation. For the Fe–PP1 complex, significant changes occurred in the 275–475 nm region with respect to the Fe(III) aquo ion (Fig. 2(a)). Two peaks at 343 and 406 nm are characteristic for the complex, with a net increase of the overall absorption coefficient.

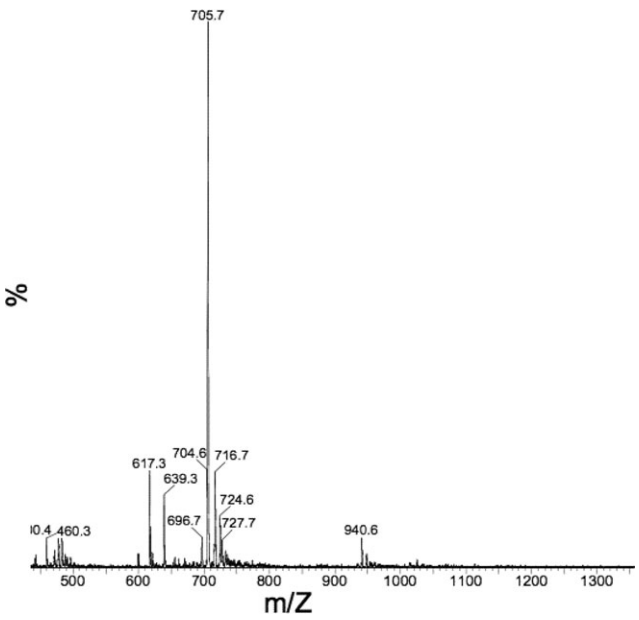

Fig. 1 Positive ion mass spectrum (ESI+/MS) of the Fe–PP1 complex.

The spectrum of Pu(IV) in nitric acid displays the characteristic absorption band at 475 nm. The addition of 1.5 equivalents of PP1 resulted in the disappearance of this specific band while two bands appeared at 457 and 515 nm (Fig. 2(b)). This suggests the formation of the Pu–PP1 complex. The absence of any precipitate and of any absorption band at 620 nm precludes the formation of hydroxide colloids.[23]

The spectrum of Np(IV) in hydrochloric acid shown in Fig. 2(c) has characteristic absorption bands at 724 and 961 nm (not shown). In the presence of 5 equivalents of PP1 the band at 724 nm disappears while a new band appears at 746 nm, suggesting the complexation of Np(IV) with PP1. The absence of any precipitate and any significant increase of the absorbance in the 400–650 nm region precludes the formation of colloidal neptunium hydroxides. In addition, the spectrum exhibits no band at 981 nm indicating that no Np(V) was produced in the solution. In order to evaluate the stoichiometry of the complex, a spectrophotometric titration was undertaken with increasing quantities of PP1 equivalents. The spectra are presented in Fig. 3(a) (corrected from dilution) and the titration curves in Fig. 3(b). For PP1 : Np molar ratios of 0.2–0.6 : 1, a yellowish white precipitate was formed, indicating that more than 0.6 equivalents of peptide is needed to chelate Np(IV) and therefore to prevent its hydrolysis into Np(IV) hydroxide. From 0.7 equivalents of peptide, with increasing quantities of peptide up to 23 equivalents the band at 746 nm remains unchanged. It can be concluded that 0.7 equivalents of peptide are enough to obtain the limit species of Np(IV)–PP1 complex, suggesting that the Np : PP1 ratio is close to 3 : 2. The comparison of UV-visible-NIR spectra of Np–PP1 with a 1 : 1 ratio at pH $\approx$1.5, $\approx$5 and $\approx$8 shows that pH has no influence on the Np–PP1 species, and that the peptide prevents the actinide to undergo hydrolysis in high pH conditions.

NMR of PP1 and Th–PP1 complex

Several sequences were used to identify and attribute the NMR signals of various atoms of the free peptide in water (Fig. 4). All ^1H and ^{13}C attributions are listed in Table 2. The gHSQC-^{13}C NMR spectrum enabled to identify the ^1H signals from –CH (between 3.3 and 4.3 ppm), $-CH_2$ (between 0.8 and 2.9 ppm), and $-CH_3$ 42 (1.02 ppm). Proton signals from $-NH_2$ (6.44 and 6.08 ppm), –CH 20 (3.4 ppm) and cyclic $-CH_2$ were identified with the gCOSY spectrum. The remaining ^1H and ^{13}C signals were attributed with a gHMBC-^{13}C spectrum, except for the non-cyclic $-CH_2$ ^1H signals, which formed a massif between 1.5 and 1.9 ppm. ^{15}N signals were attributed by means of gHMBC-^{15}N: the chemical shift of nitrogen 34 being around 471.7 ppm, while nitrogens 3, 11 and 26 appeared between 472 and 464 ppm. The cyclic nitrogen (*N-21*) was absent on the spectrum, probably because of few magnetically equivalent protons neighboring this atom and thus, the lack of transferred polarization.[24]

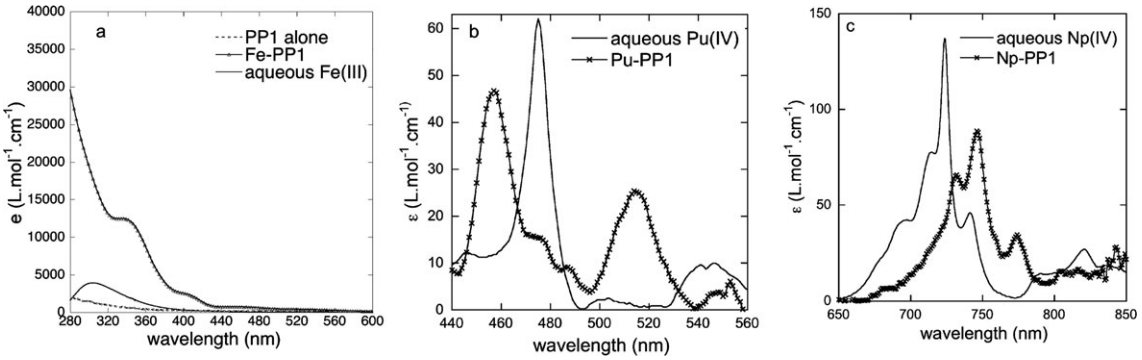

Fig. 2 Spectrophotometric spectra of (a) peptide alone in water and Fe–PP1–UV, pH = 5; (b) Pu(IV) aqua solution in 0.5 M HNO_3 and Pu–PP1; (c) Np(IV) aqua solution in HCl 1 M and Np–PP1-5.5.

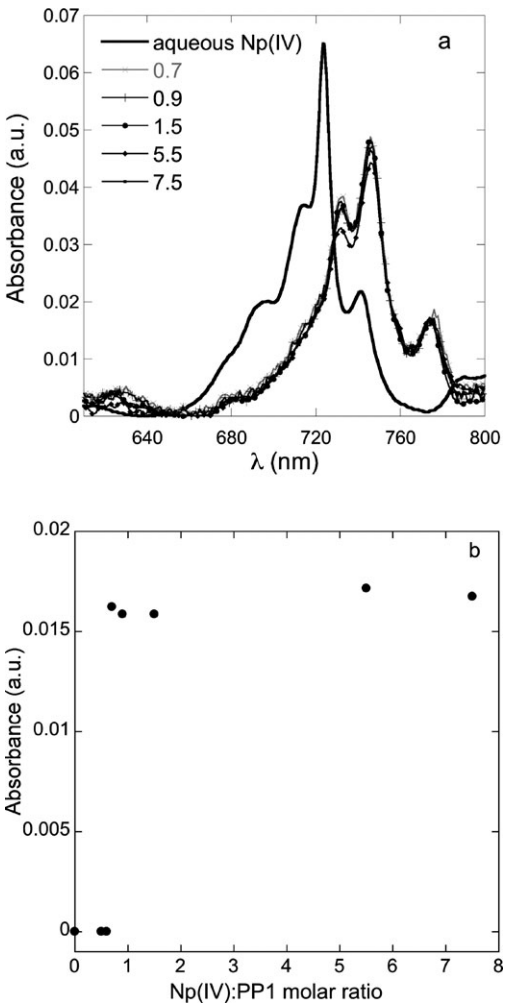

Fig. 3 (a) Spectrophotometric spectra of the Np(IV)–PP1 complex with increasing molar ratio of peptide in water + HEPES, pH ~1.5; (b) corresponding titration curve followed at 774 nm.

The chemical functions of PP1 involved in the complexation of actinides were identified by comparison of NMR spectra in the absence or presence of Th(IV) in 0.1 M HEPES in water, pH = 7. The candidate complexation sites of PP1 can be characterized with the ^{1}H spectrum, which contains information on the –NH protons from the amido-function, and the gHMBC-^{13}C spectrum, which enlightens on the –C═O

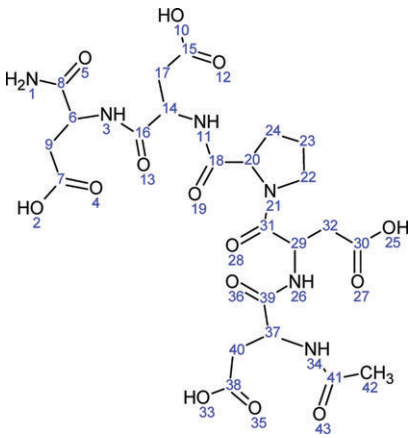

Fig. 4 Drawing of the PP1 peptide with labeling of the atoms contributing to the NMR signals described in Table 2.

carbons from amido- and carboxylato-functions. Although the concentration of HEPES was 75 times higher than that of the metal cation, the ^{1}H signals from buffering compound remained unchanged whenever thorium was present or not. This strongly suggests that Th(IV), and probably the other studied actinides, do not complex with HEPES.

No ^{1}H signals from the C-terminal amido function ($CO–NH_2$) were detectable on the gHMBC-^{13}C spectrum, either for the free PP1 or the Th–PP1 sample. This probably resulted from an exchange between these protons and the water protons, reducing their relaxation time and preventing the coupling with neighboring ^{13}C. Thus, this experiment did not allow to conclude on the role of this specific function within PP1–actinide complexes. Similarly, the role of the amido-function of the proline residue (*C-31*) could not be determined, as its correlation signal with the adjacent proton (*H-29*) was hidden by the water signal.

Comparison of the gHMBC-^{13}C spectra with and without thorium(IV) showed that all the correlation signals corresponding to the carboxylato-function (*C-7*, *-15*, *-30* and *-38*) and to the amido-functions (*C-16*, *-18*, and *-39*) were affected. Only the acetato-function (*C-41*) remained unchanged in the presence of Th(IV). Since the signal of the amido-functions were weaker than that of the carboxylato-functions in the presence of HEPES, the additional contribution of Th(IV) led to the total disappearance of the amido signal while the

Table 2 Comparative NMR spectra (δ/ppm) of free and thorium bound peptide. Attribution of ^{1}H and ^{13}C signals for specific atoms sensitive to change in the electronic environment upon Th–PP1 formation

Atom no.	$\delta(^{1}H)$ free PP1	$\delta(^{13}C)$ free PP1	$\delta(^{1}H)$ Th–PP1 complex	$\delta(^{13}C)$ Th–PP1 complex
3	7.115	—	Disappears	—
11, *26*	7.42	—	Disappears	—
34	7.295	—	Disappears	—
30	—	175	—	175
7, *15*, *38*	—	175.8–174.2	—	175.8–174.2

carboxylato signals were reduced in intensity. This can be due to the diamagnetic relaxation from Th(IV) and/or a ligand exchange leading to an additional proton relaxation time. In any case, the correlation peak modifications are related to and can only be explained by the vicinity of thorium(IV) to both the amido- and carboxylato-functions.

EXAFS

EXAFS spectra of M–PP1 (M = Fe, Th, Np, Pu) and the corresponding Fourier transforms are presented in Fig. 5(a) and (b), respectively. The pseudo-radial distribution function corresponding to the EXAFS spectra of all An–PP1 (An = Th, Np, Pu) show similar features: the first shell is split into two main contributions, and a M–M contribution clearly appears at distance >3.5 Å. Thus, one can assume that the metal–peptide complexes are at least binuclear. The first low-Z contribution of the first shell, being at a very short distance, could be attributed to μ_2-oxo or μ_2-hydroxo bridges between the actinide cations. The Fourier transform of the EXAFS spectrum of Fe–PP1 also possesses a Fe–Fe contribution around 3 Å. Therefore, despite the impossibility to qualitatively distinguish two contributions in the first shell of iron, the iron complex was considered to have the same type of structure as that of the actinide ones. Consequently, all the EXAFS spectra were adjusted in a similar way, assuming that the complexes form linear chains of $[M(\mu_2\text{-}O(H))_2(PP1)_x]$ moieties (M = Fe, Th, Np, Pu). Although dealing with different ligands, points of comparison can be made with $[Eu(tpa)(\mu_2\text{-}OH)(Otf)_2]_2$ (tpa = tris(2-pyridylmethyl)amine) forming a dimeric bridged hydroxo complex.[25] The formation of circular clusters as encountered in the structure of iron acetate[18] could not be excluded since they can not be distinguished at this point from linear ones. With this assumption in mind, and only in the case of a linear structure, the number of metal neighbors N_M has been linked in the fit to the number of short distance oxygen atoms $N_0 = 4(N-1)/N = 2N_M$, N being the complex nuclearity (*i.e.* the number of cations) if one considers a linear chain. Thus the relation between N_M and N is given by $N_M = 2(N-1)/N$. The value of N_M was restrained between 0 (monomer, $N = 1$) and 2 (infinite chain, N = infinity). It is to be noted that the error on the nuclearity becomes very large when N_M tends to 2. For instance, the error on N is 50% for $N_M = 1.25$, assuming a traditional error on amplitude factors in EXAFS fitting of about 20%. The error on N increases as a quadratic function of N_M which makes small variations of nuclearity very hazardous to estimate.

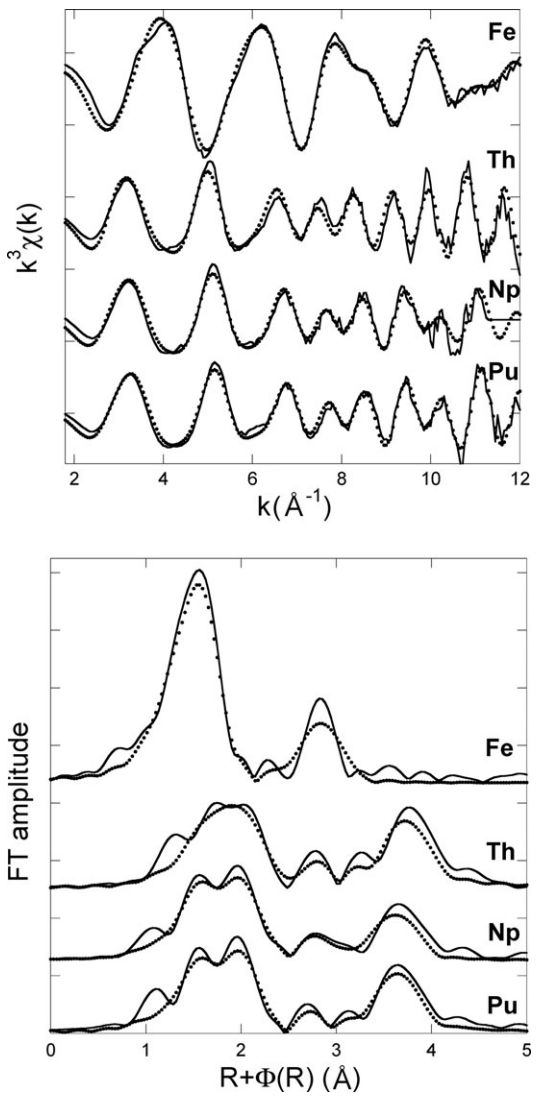

Fig. 5 Experimental (straight line) and adjusted (dotted line) EXAFS spectra (a) and Fourier transform of the EXAFS spectra (b) of samples Fe–PP1, Th–PP1, Np–PP1-1.5 and Pu–PP1.

Best fit parameters for M–PP1 samples are displayed in Table 3. It can be noticed that, whatever the sample, the first oxygen contribution is at a shorter distance than classical M–O(aquo) distances. Indeed, the M–O distance is 0.09 Å shorter for Fe–PP1 than for Fe–aquo,[26] and 0.15 and 0.17 Å shorter, respectively, in the case of Np–PP1 and Pu–PP1, compared to the corresponding aquo species.[27] This supports the assumption that μ-oxo or μ-hydroxo bridges occur.

The nuclearity of the M–PP1 complexes was estimated from N_M, as described above. Fe–PP1 nuclearity is around 2, which confirms the fact, pointed out with mass spectroscopy, that the iron complex is binuclear. Similar nuclearities were obtained for Np–PP1, Pu–PP1 and Th–PP1 with values higher than 2,

Table 3 Best fit parameters of the EXAFS spectra of Fe–PP1, Th–PP1, Np–PP1 and Pu–PP1 in water plus HEPES: σ^2 (Å^2) is the Debye–Waller factor, $S_0{}^2$ is the global amplitude factor, e_0 (eV) is the energy shift factor, r and $\Delta\chi^2{}_\nu$ are respectively the R factor and the quality factor of the fit in R space, and ε is the average noise of the spectrum in $k^3\chi(k)$. Uncertainties are given in parentheses. Numbers in italics have been linked

Sample	Neighbors	$S_0{}^2$, e_0 r factor ε, $\Delta\chi^2{}_\nu$
Fe–PP1	2.0(1) O at 1.92(1) Å, σ^2 = 0.0038 *4.0* O at 2.04(1) Å, σ^2 = 0.0032 0.8(8) C at 2.98(2) Å, σ^2 = 0.0010 *1.0* Fe at 3.30(1) Å, σ^2 = 0.0037	0.8, 2.1 1.8% 0.0011, 0,8
Th–PP1	3.9(2) O at 2.34(1) Å, σ^2 = 0.0115 *5.1* O at 2.51(1) Å, σ^2 = 0.0083 3.8(20) C at 3.09(5) Å, σ^2 = *0.0169* 6.7(30) C at 3.59(4) Å, σ^2 = *0.0169* *2.0* Th at 3.92(1) Å, σ^2 = 0.0010	1.0, −2.7 7.3% 0.0015, 2.0
Np–PP1-1.5	3.4(2) O at 2.23(1) Å, σ^2 = 0.0072 *5.6* O at 2.43(1) Å, σ^2 = 0.0064 1.4(10) C at 2.90(4) Å, σ^2 = *0.0099* 5.2(20) C at 3.47(2) Å, σ^2 = *0.0099* *1.7* Np at 3.80(1) Å, σ^2 = 0.0032	1.0, −6.1 3.3% 0.0011, 1.5
Pu–PP1	3.3(1) O at 2.22(1) Å, σ^2 = 0.0073 *5.7* O at 2.41(1) Å, σ^2 = 0.0065 3.3(14) C at 2.94(5) Å, σ^2 = *0.0228* 8.9(24) C at 3.45(3) Å, σ^2 = *0.0228* *1.7* Pu at 3.79(1) Å, σ^2 = 0.0013	1.0, −6.8 2.3% 0.0012, 0.9

Table 4 Best fit parameters for the adjustment of Np : PP1 at pH 1.5, 5 and 8. σ^2 (Å^2) is the Debye–Waller factor, $S_0{}^2$ is the global amplitude factor, e_0 (eV) is the energy shift factor, r and $\Delta\chi^2{}_\nu$ are respectively the R factor and the quality factor of the fit in R space, and ε is the average noise of the spectrum in $k^3\chi(k)$. Uncertainties are given in parentheses. Numbers in italics have been fixed or linked

Sample	Neighbours	$S_0{}^2$, e_0 r factor ε, $\Delta\chi^2{}_\nu$
Np–PP1-1.5	3.4(2) O at 2.23(1) Å, σ^2 = 0.0072 *5.6* O at 2.43(1) Å, σ^2 = 0.0064 1.4(10) C at 2.90(4) Å, σ^2 = *0.0099* 5.2(20) C at 3.47(2) Å, σ^2 = *0.0099* *1.7* Np at 3.80(1) Å, σ^2 = 0.0032	1.0, −6.1 3.3% 0.0011, 1.5
Np–PP1-7.5	3.5(2) O at 2.24(1) Å, σ^2 = 0.0088 *5.5* O at 2.43(1) Å, σ^2 = 0.0073 2.5(12) C at 2.93(5) Å, σ^2 = *0.0172* 6.6(22) C at 3.47(3) Å, σ^2 = *0.0172* *1.8* Np at 3.81(1) Å, σ^2 = 0.0035	1.1, −5.5 4.2% 0.0011, 2.2
Np–PP1-23	3.5(2) O at 2.25(1) Å, σ^2 = 0.0085 *5.5* O at 2.44(1) Å, σ^2 = 0.0073 3.2(14) C at 2.91(3) Å, σ^2 = *0.0161* 4.8(20) C at 3.46(4) Å, σ^2 = *0.0161* *1.7* Np at 3.81(1) Å, σ^2 = 0.0031	0.9, −5.5 3.7% 0.0008, 2.4
Np–PP1-pH5	3.6(2) O at 2.24(1) Å, σ^2 = 0.0070 *5.4* O at 2.43(1) Å, σ^2 = 0.0062 2.4(13) C at 2.92(5) Å, σ^2 = *0.0179* 6.8(22) C at 3.48(3) Å, σ^2 = *0.0179* *1.8* Np at 3.80(1) Å, σ^2 = 0.0023	1.0, −6.2 3.8% 0.0010, 1.9
Np–PP1-pH8	3.8(2) O at 2.25(1) Å, σ^2 = 0.0071 *5.2* O at 2.44(1) Å, σ^2 = 0.0068 3.0(13) C at 2.91(5) Å, σ^2 = *0.0176* 5.6(23) C at 3.49(4) Å, σ^2 = *0.0176* *1.9* Np at 3.81(1) Å, σ^2 = 0.0030	0.9, −5.7 4.3% 0.0010, 1.8

suggesting that the complexes form oligomeric chains. However the exact value of nuclearity is difficult to estimate (see above) and no significant differences were observed between Th, Np and Pu.

One shell of carbon atoms was necessary for the fitting of the Fe–PP1 EXAFS spectra whereas two shells of carbon atoms were required to obtain a satisfactory adjustment of the Th–PP1, Np–PP1 and Pu–PP1 EXAFS spectra. One can note that for Th–PP1, Np–PP1 and Pu–PP1, the Debye–Waller factors of both carbon atom shells are abnormally high ($\sim$0.01–0.02 Å^2) as well as the error on coordination numbers. Similarly, the error on corresponding distances is higher than for the other distances. Although necessary, the contributions of the carbon shells remain fuzzy from the EXAFS point of view. This is probably related to the flexibility of the peptide chain and the difficulty to define one type of carbon contribution. The number of neighbors fitted for these shell should therefore be considered with a lot of caution.

The influence of pH and of the actinide : PP1 ratio has also been investigated. Consequently, the EXAFS spectra of Np-PP1 samples at adjusted pH = 1.5, 5 and 8 with 1 : 1.5 ratio, and at pH = 1.5 with 1 : 1.5, 1 : 7.5 and 1 : 23 ratios were recorded. Best fit parameters are displayed in Table 4. In agreement with the UV-visible-NIR experiments, no major difference was observed between spectra, showing that, whatever the pH and the An : peptide ratio, the formed species mostly remain the same.

Discussion

The combination of all the above spectroscopic data strongly suggests that the interaction of PP1, Ac–AspAspProAspAsp–NH_2, with Fe(III), Th(IV), Np(IV) and Pu(IV) cations relies on a original type of peptidic complexes. The formation of such molecular species prevents the actinide and iron cations from the hydrolysis that usually occurs under comparable conditions. Indeed, close inspection of the Np and Pu spectrophotometric data in the UV range and in particular no increase of the absorbance in the 400–650 nm region permits to rule out the formation of soluble and insoluble hydroxide colloids. This is further confirmed by the EXAFS structural parameters of the four complexes. However, the M–PP1 complexes share some structural similarities with products of iron and actinide hydrolysis such as $[Th_2(\mu_2\text{-}OH)_2(NO_3)_6(H_2O)_6]\cdot H_2O$, $[Th(\mu_2\text{-}OH)_2Cl_2(H_2O)_{12}]Cl_4$,[28] $NH_4Np(OH)_5$[29] or Pu hydrolysis products described by Denecke *et al.*[30] and Conradson *et al.*:[31] a first short M–O distance, and M–M interactions.

The first M–O oxygen distance of M–PP1 complexes are in the same range as the first M–O distance of hydrolysis products. For instance, for $[Th_2(\mu_2\text{-}OH)_2(NO_3)_6(H_2O)_6]\cdot H_2O$ and $[Th(\mu_2\text{-}OH)_2Cl_2(H_2O)_{12}]Cl_4$, d_{Th-O} = 2.36 Å. Regarding Pu(IV) hydrolysis products, d_{Pu-O} range between 2.20 and 2.22 Å. In $NH_4Np(OH)_5$, although very disperse, the Np–OH distances average at 2.33 Å. These distances are very similar to 2.33, 2.32 and 2.22 Å in M–PP1 (M = Th, Np, Pu, respectively) complexes. Consequently, the first oxygen shell can be attributed to μ-hydroxo or μ-oxo

oxygen atoms. However, significant differences appear. Notably, the M–M distance in M–PP1 complexes are significantly shorter than those in the hydrolysis products: $\Delta(d^{\mathrm{Coll}}_{\mathrm{Th-Th}} - d^{\mathrm{ThPP1}}_{\mathrm{Th-Th}}) = 0.08$–$0.10$ Å $\Delta(d^{\mathrm{Np(OH)}_5^-}_{\mathrm{Np-Np}} - d^{\mathrm{NpPP1}}_{\mathrm{Np-Np}}) = 0.1$ Å and $\Delta(d^{\mathrm{Coll}}_{\mathrm{Pu-Pu}} - d^{\mathrm{PuPP1}}_{\mathrm{Pu-Pu}}) = 0.06$–$0.08$ Å. To our knowledge, no further data are available for direct comparison with Fe(III) hydroxides although a double μ-O, μ-OH bridge complex has been reported.[32] In this complex, the average Fe(III)-μ–OH bond distance is equal to 1.99 Å, the Fe(III)-μ–O bond distance to 1.87 Å and the Fe(III)–Fe(III) distance to 2.87 Å. The later distance deviates significantly from our results and this may be due to the distortion of the bridge.

The EXAFS data also show a second shell of oxygen atoms, which can be attributed to the peptide interaction with the cation. According to the NMR study, this interaction occurs through the carboxylato functions and vicinity of the amido functions of the peptide bounds in a way that is not fully understood yet. Note that the carboxylato oxygen atoms of the peptide, as hard bases, usually interact with hard acids such as iron(III) or actinide(IV). However, our experimental conditions might be too acidic for a complete deprotonation of the carboxylic functions ($pK_{aPP1} \sim 4.4$), leading to possible exchange with the solvent.

The difference in nuclearity between iron on the one hand and actinides on the other hand led us to conclude on different types of species. Indeed, Fe–PP1 forms a dimeric complex, also suggested by mass spectrometry. On the other hand, the actinide–PP1 complexes occur as edifices of higher nuclearity.

In parallel, molecular dynamics simulations with constraints of experimental distances were performed for the PP1–2Fe^{3+} (Fe^{3+})$_2$–PP1 system at the 2 : 1 stoichiometry. Molecular dynamics trajectories obtained for the peptide with all the aspartic carboxylates that are protonated first indicated that PP1 was able to adopt two different conformations around the ionic system: (i) a mostly extended conformation close to polyproline and (ii) a folded β-turn conformation encompassing the Asp2–Pro3–Asp4–Asp5 residues (see Fig. 6(a)). In all cases but two, the two polyproline and β-turn conformations were retrieved in equilibrium. The two other cases are (i) Asp1/Asp4 couple complexing both Fe^{3+} ions and for which only the polyproline conformation was observed; (ii) Asp1/Asp5 couple mostly favoring the formation of the β-turn conformation. Examining the internal energy of the peptide along the obtained trajectories argued for a better stability of the β-turn conformation. The quasi-extended polyproline conformation indeed led to possible repulsions of the Asp side chains. Interestingly, closely related conclusions were drawn from the simulations in which the two remaining Asp residues (not complexing the Fe^{3+} ions) were protonated. After energy minimization of the most representative structures extracted from these trajectories, it was observed that the β-turn conformation was the same and independent of the choice of the two Asp residues complexing both Fe^{3+}. This suggests a preferred orientation of the peptide around the ionic system (see Fig. 6(b)).

Simulations performed with the same protocol on the isolated PP1 peptide also led to an equilibrium between these two conformations. Actually, it is hard to quantitatively determine

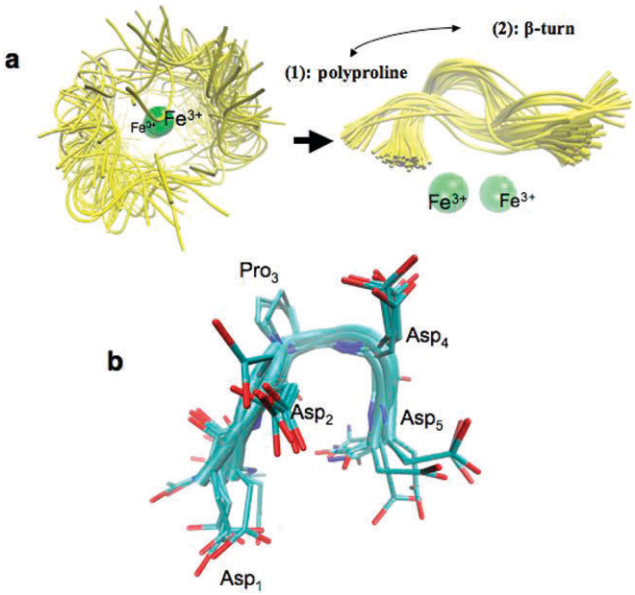

Fig. 6 Analysis of the molecular dynamics simulations performed for the PP1–2Fe^{3+} system, Asp2/Asp5 complexing Fe^{3+}. (a) After a structural fit on the peptide backbone atoms, models compatible with the experimental distances constraints included a quasi-extended polyproline like conformation and a Asp2–Pro3–Asp4–Asp5 β-turn; (b) the same β-turn conformation was retrieved in all simulations except for the Asp1/Asp4 couple.

if the equilibrium may be displaced towards the β-turn conformation in the (Fe^{3+})$_2$–PP1 complex, as the simulations have all been performed *in vacuo*. Nevertheless, and as expected, the unbound peptide was qualitatively more flexible than the peptide bound to Fe^{3+} arguing for more β-turn in the (Fe^{3+})$_2$–PP1 system.

Finally, a 3D statistical calculation was performed which aim was to determine the most favorable orientations of the peptide around the ionic system. For each independent trajectory, the method consisted to fit all the obtained snapshots on the Fe^{3+} ions and then to statistically analyze all the resulting positions of the peptide through atomic densities maps in 3D. Visualization of these maps in 3D using increasing threshold values lead to statistically equivalent positions of the peptide around the ionic system. For each independent trajectory, these analyses revealed the possibility to place two copies of PP1 around both Fe^{3+} ions without any steric clash (Fig. 7(a)), and in agreement with the experimental observations. Such a model is represented in Fig. 7(b) in which each Fe^{3+} interacts with two Asp residues. For instance in the depicted case Asp1 and Asp2, the β-turn conformation of the peptide brings the C-terminal amide groups at a distance compatible with H-bonding with the two hydroxyl ions, also in agreement with experimental data. Although the results of these theoretical calculations may not be considered as quantitative, they already allow to propose a 3D orientation of both peptide copies around the two Fe^{3+} cations that are in full agreement with the EXAFS data. Furthermore, one can propose a similar model with An(IV) cations in which the peptide chains are engaged in a polynuclear complex. The differences in complex nuclearities observed by EXAFS

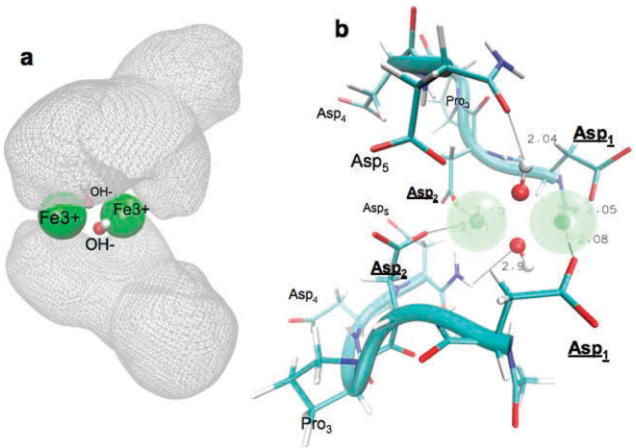

Fig. 7 (a) 3D volumetric densities maps of the peptide around the Fe^{3+}/OH^{-} ionic system which demonstrated, for a same threshold value, the possibility to place two copies of the β-turn folded peptide without any steric clash. (b) Model in which Asp1 and Asp2 are complexing the Fe^{3+} cations; the folding of the peptide allows an additional H-bond between both the C-terminal amide groups and the two OH^{-} bridges.

between iron on one side, neptunium, plutonium and thorium on the other side are not fully understood at this point and will be the subject of further efforts.

Conclusion

The relative lack of structural data for biochemical complexes of actinides was at the origin of this work. Our reductionist approach permitted to collect data for several cations, among which Th(IV), Np(IV) and Pu(IV) cations. Fe(III) was also investigated since it is frequently claimed that actinides exhibit comparable chelation properties, and even affinity, towards iron-binding proteins.

Np and Pu complexes provide with striking examples of how a peptide chelate can prevent hydrolysis of the metal cation into insoluble hydroxide species. Both mass spectrometry and EXAFS at the iron K edge concluded on the fact that the iron complex displays a peculiar diferric structure. EXAFS data at the actinide L_{III} edge indicated that polynuclear species could be obtained for actinides too. NMR and EXAFS allowed the description of a molecular scheme for these complexes where all cations get linked by hydroxo or oxo bridges and where the peptide ligand fills the cation coordination sphere.

In addition, molecular dynamics calculations on the $(Fe^{3+})_2$–PP1 complex confirmed the involvement of the peptide conformation. A β-turn conformation was proposed to give a better stability. Some data suggests a preferred orientation of the peptide around the ionic system. Finally, a 3D statistical analysis revealed the possibility to place two PP1 around both Fe^{3+} ions without any steric hindrance. One can then propose a similar model with An(IV) cations in which the peptide chains are engaged in a polynuclear complex.

Acknowledgements

This work was supported by the French Environmental Toxicology Program and CEA/DEN/DDIN/MR. XAS measurements were carried out at ESRF, a European user facility, and at Stanford Synchrotron Radiation Laboratory, a national user facility operated by Stanford University on behalf of the US department of Energy, Office of Basic Energy Sciences. The authors thank C. J. Bargar and J. Rogers (SSRL/11-2), and S. D. Conradson (LANL) for their help.

References

1 E. Ansoborlo, O. Prat, P. Moisy, C. Den Auwer, P. Guilbaud, M. Carriere, B. Gouget, J. Duffield, D. Doizi, T. Vercouter, C. Moulin and V. Moulin, *Biochimie*, 2006, **88**, 1605.
2 A. E. Gorden, J. Xu, K. N. Raymond and P. Durbin, *Chem. Rev.*, 2003, **103**, 4207.
3 M. P. Neu, in *Advances in Plutonium Chemistry 1967–2000*, ed. D. C. Hoffman, Am. Nucl. Soc., 2002, p. 169.
4 H. Li, P. J. Sadler and H. Sun, *Eur. J. Biochem.*, 1996, **242**, 387.
5 Z. Szabó, T. Toraishi, V. Vallet and I. Grenthe, *Coord. Chem. Rev.*, 2006, **250**, 784.
6 G. Grossmann, M. Neu, E. Pantos, F. J. Schwab, R. W. Evans, E. Townes-Andrews, P. F. Lindley, H. Appel, W.-D. Thies and S. S. Hasnain, *J. Mol. Biol.*, 1992, **225**, 811.
7 P. A. Seeger, S. E. Rokop, P. D. Palmer, S. J. Henderson, D. E. Hobart and J. Trewhella, *J. Am. Chem. Soc.*, 1997, **119**, 5118.
8 J. D. Van Horn and H. Huang, *Coord. Chem. Rev.*, 2006, **250**, 765.
9 O. Pible, P. Guilbaud, J.-L. Pellequer, C. Vidaud and E. Quéméneur, *Biochimie*, 2006, **88**, 1631.
10 T. Hayashi, T. Asai and H. Ogoshi, *Tetrahedron Lett.*, 1997, **38**, 3039.
11 S. M. Cowell, Y. S. Lee, J. P. Cain and V. J. Hruby, *Curr. Med. Chem.*, 2004, **11**, 2785.
12 M. Kilyén, Péter Forgo, A. Lakatos, G. Dombi, T. Kiss, N. Kotsakis and A. Salifoglou, *J. Inorg. Biochem.*, 2003, **94**, 207.
13 I. Ascone, R. Fourme, S. Hasnain and K. Hodgson, *J. Synchrotron Radiat.*, 2005, **12**, 1.
14 S. S. Hasnain and R. W. Strange, *J. Synchrotron Radiat.*, 2003, **10**, 9.
15 B. Ravel and M. Newville, *J. Synchrotron Radiat.*, 2005, **12**, 537.
16 A. Michalowicz, EXAFS code available at http://icmpe.cnrs.fr.
17 J. J. Rehr and R. C. Albers, *Rev. Mod. Phys.*, 2000, **72**, 621.
18 K. I. Turte, S. G. Shova, F. A. Spatar, M. D. Mazus and T. I. Malinovskii, *J. Struct. Chem.*, 1994, **35**, 248.
19 G. G. Sadikov, G. A. Kukina, M. A. Porai-Koshits and L. A. Pospelova, *J. Struct. Chem.*, 1968, **9**, 128.
20 B. R. Brooks, R. E. Bruccoleri, B. D. Olafson, D. J. States, S. Swaminathan and M. Karplus, *J. Comput. Chem.*, 1983, **4**, 187.
21 A. D. MacKerell, D. Bashford, M. Bellott, R. L. Dunbrack, J. D. Evanseck, M. J. Field, S. Fischer, J. Gao, H. Guo, S. Ha, D. Joseph-McCarthy, L. Kuchnir, K. Kuczera, F. T. K. Lau, C. Mattos, S. Michnick, T. Ngo, D. T. Nguyen, B. Prodhom, W. E. Reiher, B. Roux, M. Schlenkrich, J. C. Smith, R. Stote, J. Straub, M. Watanabe, J. Wiorkiewicz-Kuczera, D. Yin and M. Karplus, *J. Phys. Chem. B*, 1998, **102**, 3586.
22 W. Humphrey, A. Dalke and K. Schulten, *J. Mol. Graph.*, 1996, **14**, 33.
23 C. Walther, H. R. Cho, C. M. Marquardt, V. Neck, A. Seibert, J. I. Yun and Th. Fanghänel, *Radiochim. Acta*, 2007, **95**, 7.
24 H. Kessler, W. Hehlein and R. Schuck, *J. Am. Chem. Soc.*, 1982, **104**, 4534.
25 L. Natrajan, J. Pécaut, M. Mazzanti and C. LeBrun, *Inorg. Chem.*, 2005, **44**, 4756.
26 P. D'Angelo and M. Benfatto, *J. Phys. Chem. A*, 2004, **108**, 4505.
27 M. R. Antonio, L. Soderholm and C. W. Williams, *Radiochim. Acta*, 2001, **89**, 17.
28 R. E. Wilson, S. Skanthakumar, G. Sigmon, P. C. Burns and L. Soderholm, *Inorg. Chem.*, 2007, **46**, 2368.
29 A. Cousson, H. Abazli, F. Nectoux, J. Jové and M. Pagès, *J. Less Common Met.*, 1986, **121**, 405.
30 J. Rothe, C. Walther, M. A. Denecke and T. Fanghänel, *Inorg. Chem.*, 2004, **43**, 4708.
31 S. D. Conradson, *Appl. Spectrosc.*, 1998, **52**, 252A.
32 A. Stubna, D.-H. Jo, M. Costas, W. W. Brenessel, H. Andres, E. L. Bominaar, E. Munck and L. Que, Jr, *Inorg. Chem.*, 2004, **43**, 3067.